Article

Cell Reports

Microtubule Destabilizer KIF2A Undergoes Distinct Site-Specific Phosphorylation Cascades that Differentially Affect Neuronal Morphogenesis

Graphical Abstract

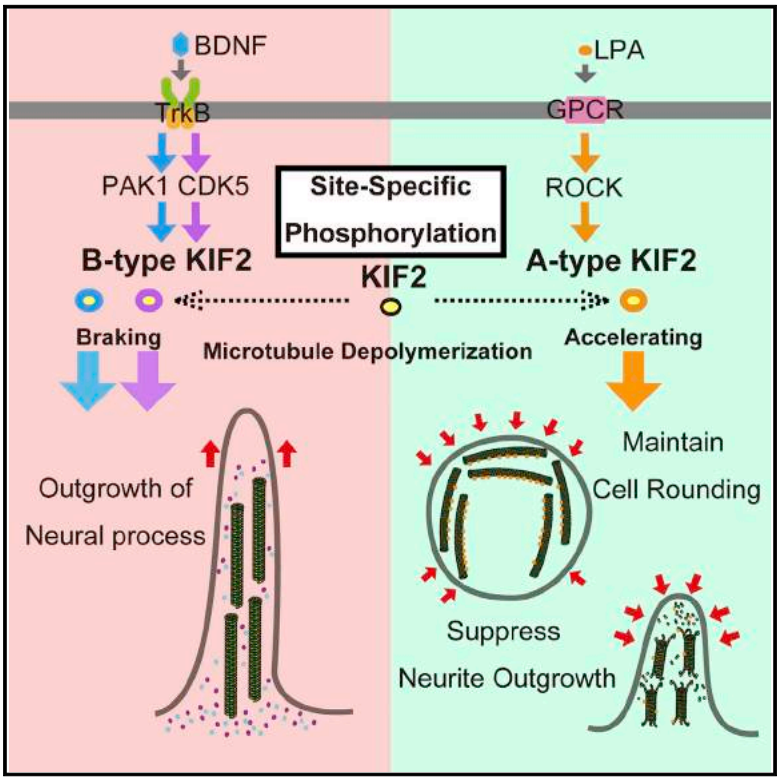

Authors

Tadayuki Ogawa, Nobutaka Hirokawa

Correspondence

hirokawa@m.u-tokyo.ac.jp

In Brief

Ogawa and Hirokawa identify two different sets of phosphorylation profiles of the microtubule destabilizer KIF2A that accelerate (A-type) and brake (B-type) the microtubule depolymerization activity of KIF2A within neurons in response to extracellular signals.

Highlights

- KIF2A undergoes two different phosphorylation cascades, A-type and B-type
- PAK1 and CDK5 induce B-type KIF2A to impede microtubule depolymerization
- ROCK2 induces A-type KIF2A to accelerate microtubule depolymerization
- A- and B-types of KIF2A phosphorylation respond to extracellular signals in neurons

Ogawa & Hirokawa, 2015, Cell Reports *12*, 1774–1788
September 22, 2015
http://dx.doi.org/10.1016/j.celrep.2015.08.018

CellPress

OPEN ACCESS
CellPress

Cell Reports
Article

Microtubule Destabilizer KIF2A Undergoes Distinct Site-Specific Phosphorylation Cascades that Differentially Affect Neuronal Morphogenesis

Tadayuki Ogawa[1] and Nobutaka Hirokawa[1,2,*]
[1]Department of Cell Biology and Anatomy, Graduate School of Medicine, University of Tokyo, Hongo, Bunkyo-ku, Tokyo 113-0033, Japan
[2]Center of Excellence in Genome Medicine Research, King Abdulaziz University, Jeddah 21589, Saudi Arabia
*Correspondence: hirokawa@m.u-tokyo.ac.jp
http://dx.doi.org/10.1016/j.celrep.2015.08.018

SUMMARY

Neurons exhibit dynamic structural changes in response to extracellular stimuli. Microtubules (MTs) provide rapid and dramatic cytoskeletal changes within the structural framework. However, the molecular mechanisms and signaling networks underlying MT dynamics remain unknown. Here, we have applied a comprehensive and quantitative phospho-analysis of the MT destabilizer KIF2A to elucidate the regulatory mechanisms of MT dynamics within neurons in response to extracellular signals. Interestingly, we identified two different sets of KIF2A phosphorylation profiles that accelerate (A-type) and brake (B-type) the MT depolymerization activity of KIF2A. Brain-derived neurotrophic factor (BDNF) stimulates PAK1 and CDK5 kinases, which decrease the MT depolymerizing activity of KIF2A through B-type phosphorylation, resulting in enhanced outgrowth of neural processes. In contrast, lysophosphatidic acid (LPA) induces ROCK2 kinase, which suppresses neurite outgrowth from round cells via A-type phosphorylation. We propose that these two mutually exclusive forms of KIF2A phosphorylation differentially regulate neuronal morphogenesis during development.

INTRODUCTION

Cells respond to a diverse array of extracellular stimuli to survive and properly develop in a dynamic environment. Neurons are highly polarized cells with extensions of long leading processes, and they exhibit dynamic structural changes in response to stimuli. Microtubules (MTs) are the key components that provide rapid and dynamic responses in the structural framework of cells; therefore, they must be controlled via specific regulatory mechanisms.

Kinesin superfamily protein 2A (KIF2A), a member of the Kinesin-13 family, is a central regulator of the MT cytoskeleton in neurons. The kinesin superfamily proteins (KIFs) are classified by the position of the catalytic domain and specific sequences (Hirokawa, 1997, 1998; Lawrence et al., 2004; Miki et al., 2001). Most KIFs move along MTs to transport cargoes (Hirokawa, 1998; Hirokawa et al., 2010); in contrast, the Kinesin-13 family proteins depolymerize MTs. Proteins of the Kinesin-13 family are divided into four sub-families: KIF2A, KIF2B, KIF2C/MCAK, and KIF24. KIF2 proteins were originally discovered in neuronal (Aizawa et al., 1992; Noda et al., 1995) and mitotic cells (Wordeman and Mitchison, 1995) and are characterized as MT destabilizers (Desai et al., 1999; Walczak et al., 1996). KIF2 proteins depolymerize MTs using class-specific structural features (Ogawa et al., 2004; Shipley et al., 2004). In cell-cycle events, KIF2 proteins function as spindle regulators (Walczak et al., 1996; Wordeman and Mitchison, 1995), and a few Aurora-kinase-dependent phosphorylation sites are reported to affect their activity (Lan et al., 2004; Ohi et al., 2004). KIF2A is enriched in developing neurons (Noda et al., 1995), and *Kif2a*$^{-/-}$ neurons show extended branches (Homma et al., 2003). Therefore, we hypothesize that there is a well-organized mechanism of controlling KIF2A activity to regulate MT dynamics and neuron morphology in response to extracellular signals. To perform comprehensive and quantitative investigations of MT regulators, we linked the conventional qualitative analysis with systematic quantitative analysis utilizing cutting-edge phospho-proteomic tools and outlined the critical phosphorylation events in KIF2A. First, we completely mapped the KIF2A phosphorylation sites and identified the specific kinases for each site. Furthermore, we quantified the site-specific phosphorylation of KIF2A in stimulated neurons. Stimulation-resistant mutagenesis affects the depolymerizing activity of KIF2A, resulting in the reversal of the neural process phenotype under stimulation. Here, we demonstrate that there is a finely regulated mechanism of controlling KIF2A activity via specific phosphorylation to transform normal KIF2A into "accelerating" KIF2A (A-type KIF2A) or "braking" KIF2A (B-type KIF2A), thus regulating MT dynamics and neuron morphology in response to extracellular signals.

RESULTS

KIF2A Is Highly Phosphorylated in the Brain

We first tested whether KIF2A is phosphorylated in the brain. Mouse brain lysates were analyzed by comparing conventional western blotting (WB) and Phos-tag WB (Kinoshita et al., 2006)

using an anti-KIF2A monoclonal antibody. Phos-tag WB showed apparent band shifts, indicating the phosphorylation of KIF2A in the brain (Figure 1B). To further investigate the phosphorylation, the digested peptides from the immuno-precipitated KIF2A (Figure S1A) were analyzed using MALDI-TOF. The spectra displayed multiple phosphorylation-specific 80-Da peak shifts compared to the control (Figure 1C). To further dissect this, the KIF2A phospho-peptides were applied to the liquid chromatography-tandem mass spectrometry (LC-MS/MS) system. We obtained more than 84% sequence coverage of KIF2A (Figure S1B), identifying at least 16 phosphorylation sites (Figures 1A, 1D, and S1C). Interestingly, the phosphorylation sites were conserved in the Kinesin-13 family across species and were located within the "KIF2Acore" domain that is critical for MTs depolymerization activity (Figure 1A). These results indicate the significance of the phosphorylation sites for KIF2 function in MT regulation via specific signaling cascades.

KIF2A Undergoes A- or B-type Phosphorylation In Vitro

To determine the KIF2A-specific signaling pathways in neurons, we next sought to identify the direct upstream kinases responsible for each phosphorylation site within the KIF2Acore. The recombinant KIF2Acore protein was applied to the "Kinome-wide" kinase assay and analyzed using Phos-tag PAGE and MALDI-TOF. Approximately 50 major neuronal kinases out of more than 500 kinases identified within the Human Genome Project were used in the assay.

Compared to the negative control, the phospho-proteins showed stoichiometric upward shifts of the bands on Phos-tag PAGE (Figure 2A). AKT1, AKT2, AuroraA, AuroraB, CaMK2A, CDK5/p25, CDK5/p35, IKKβ, MLK3, PAK1, PKA, PKCα, PKCδ, PGK, PGK2, ROCK1, ROCK2, and RSK1 showed substantial band shifts, indicating their preferential phosphorylation of KIF2A in vitro. Strikingly, CDK5, PAK1, PKA, and PKCα phosphorylated KIF2A in high stoichiometric ratios (Figure 2A). The proteins were further analyzed using MALDI-TOF, and the numbers of phosphorylation sites were roughly estimated. The phosphorylated KIF2Acore protein showed strong peak shifts, which showed an increase in the *m/z* value of 80 (HPO_3^-), which was derived from one phosphorylation (Figures 2B and S1D). Both observations suggest that these are the upstream kinases most likely to be responsible for KIF2A phosphorylation.

Because kinases target specific positions, we investigated the specific kinases responsible for each phosphorylation site on KIF2A. To date, the kinases and the phosphorylation sites have mainly been investigated using exploratory qualitative approaches. However, qualitative phosphorylation data sometimes produce vague results because of low abundance, ion suppression, and handling errors. To reveal the "true positive" specific phosphorylation by overcoming the problems of qualitative analyses, we used two independent quantitative approaches based on LC-MSn: Tandem Mass Tag (TMT) and multiple reaction monitoring (MRM, or selective reaction monitoring) (Picotti et al., 2010; Walther and Mann, 2010). The basic strategies are described in Figure S2. The kinase-specific increase in the phospho-peptides for each sample was independently quantified using a specific mass spectrometer (Figures 2C–2G, S3, and S4).

As expected, many phosphorylation sites were identified as specific targets of PAK1. Two adjoining threonines, T186/T187, and another three adjoining Ser/Thr residues, T439/S440/S441, S479 and S488 were phosphorylated by PAK1 (Figures 2D and S3A). All of these phosphorylated residues fell within the putative conserved PAK1 sequence, xRx(x)S/T. CDK5, a typical proline-directed kinase, phosphorylated T474 and S503 (Figures 2C and S3B). ROCK, a basophilic kinase that targets R/K(R/K)xS/T motifs, preferentially phosphorylated T482 (Figures 2E and S4A). IKKβ, an acidophilic kinase, phosphorylated S255 and S456 (Figures 2G and S4C). T219, T245, and S300 were preferentially phosphorylated by MLK3 (Figures 2F and S4B), and S222 was phosphorylated by CaMK2A (Figure S4D). Together, these results conclusively indicate that site-specific phosphorylation of KIF2A was introduced independently by specific kinases in vitro (summarized in Figure 1A).

B-type Phosphorylation by PAK1/CDK5 Inhibits the MT Depolymerization Activity of KIF2A

We next investigated the direct effects of phosphorylation on the KIF2A function using a sedimentation-based MT depolymerization assay in vitro. To exclude the false contribution from mutations, we used KIF2Acore proteins that were phosphorylated by different kinases. Note that the phosphorylation efficiency of KIF2Acore was different dependent on the kinase used (Figure 2A). MT depolymerization by PAK1-KIF2Acore was significantly decreased compared to the unphosphorylated wild-type (WT)-KIF2Acore (Figure 3A). Using CDK5, IKKβ, CaMK2A, and MLK3, the half-phosphorylated KIF2Acore showed decreased MT depolymerization activities. Interestingly, ROCK-KIF2Acore, which was 90% phosphorylated by ROCK2, retained MT depolymerization activity (Figures 3A and 3B). PAK1-KIF2Acore displayed a 4-fold reduction in the EC_{50} for MT depolymerization (70 nM) in relation to WT-KIF2Acore (18 nM), which indicated significantly reduced MT depolymerization activity (Figure 3B).

To examine the activity under physiological conditions, we next performed the MT depolymerizing assay (Maney et al., 2001; Ogawa et al., 2004) in COS-7 cells. For the assays, site-directed mutagenesis of full-length (FL) mouse KIF2A was performed, replacing Ser/Thr with Ala for the kinase-resistant mutants and replacing Ser/Thr with Glu for the phospho-mimetic mutants (Figure S5). PAK1-specific mutations were divided into three independent groups: neck, Loop11, and alpha5. The mutants were overexpressed in COS-7 cells, and the remaining MTs were observed. Note that the MT depolymerizing activity of WT KIF2A FL was approximately one-third the level of that of KIF2C, and the MTs remained in the cell (Figures 3C and 3D), as we previously reported (Ogawa et al., 2004).

Surprisingly, CDK5-resistant KIF2A (CDK5-res.A), T474A/S503A, showed MT depolymerizing activity that was approximately twice that of the WT KIF2A, whereas the CDK5-specific phospho-mimetic KIF2A (CDK5-phos.E), T474E/S503E, showed significantly suppressed activity (Figures 3C and 3D). The three PAK1 resistant mutants, T186A/T187A on the neck (PAK1-res.NeckA), T439A/S440A/S441A on Loop11 (PAK1-res.L11A), and S479A/S488A on alpha5 (PAK1-res.α5A), each showed activity at least as strong as WT. When all of the residues in the three groups were mutated simultaneously (PAK1-res.allA),

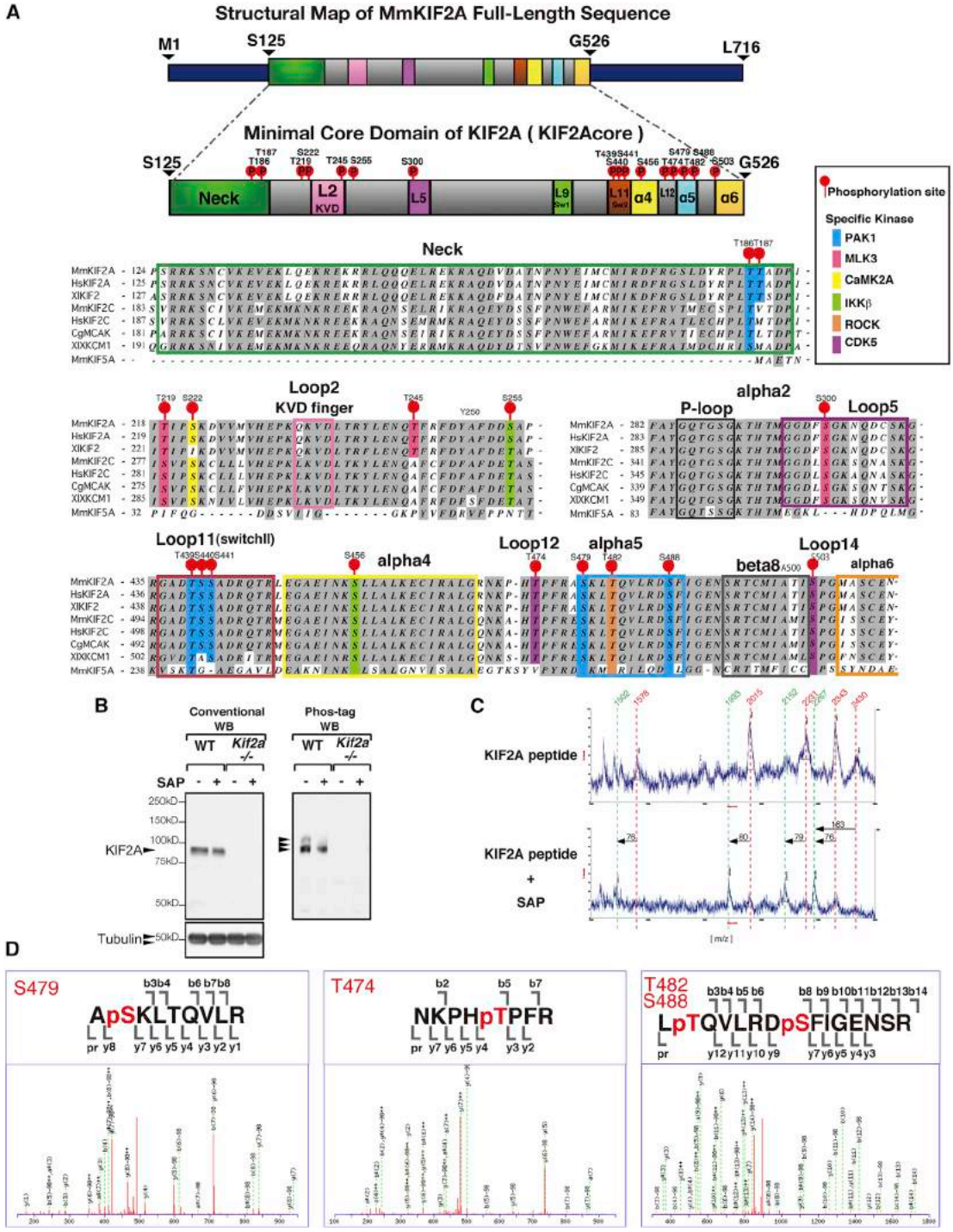

Figure 1. Phosphorylation of KIF2A in Mouse Brain

(A) Phosphorylation map of mouse KIF2A. MmKIF2A is aligned with Kinesin-13 family proteins. KIF5A is provided for comparison. KIF2-specific sequences are enclosed in colored boxes that correspond to specific structures. The phosphorylation sites are indicated by red flags, and the conserved sites are shown with colored backgrounds. The background colors correspond to the kinases.

(B) KIF2A is phosphorylated in the brain. Mouse brain lysates were analyzed by conventional WB and Phos-tag WB using anti-KIF2A monoclonal antibody. The lysate treated with shrimp alkaline phosphatase (SAP) was applied as a negative control. α-Tubulin was blotted as a loading control.

(C) The MALDI-TOF spectra of the native KIF2A phospho-peptides show multiple phosphorylation-specific peak shifts compared to the SAP-treated peptides.

(D) Typical MS/MS spectrum of KIF2A phospho-peptides.

See also Figure S1.

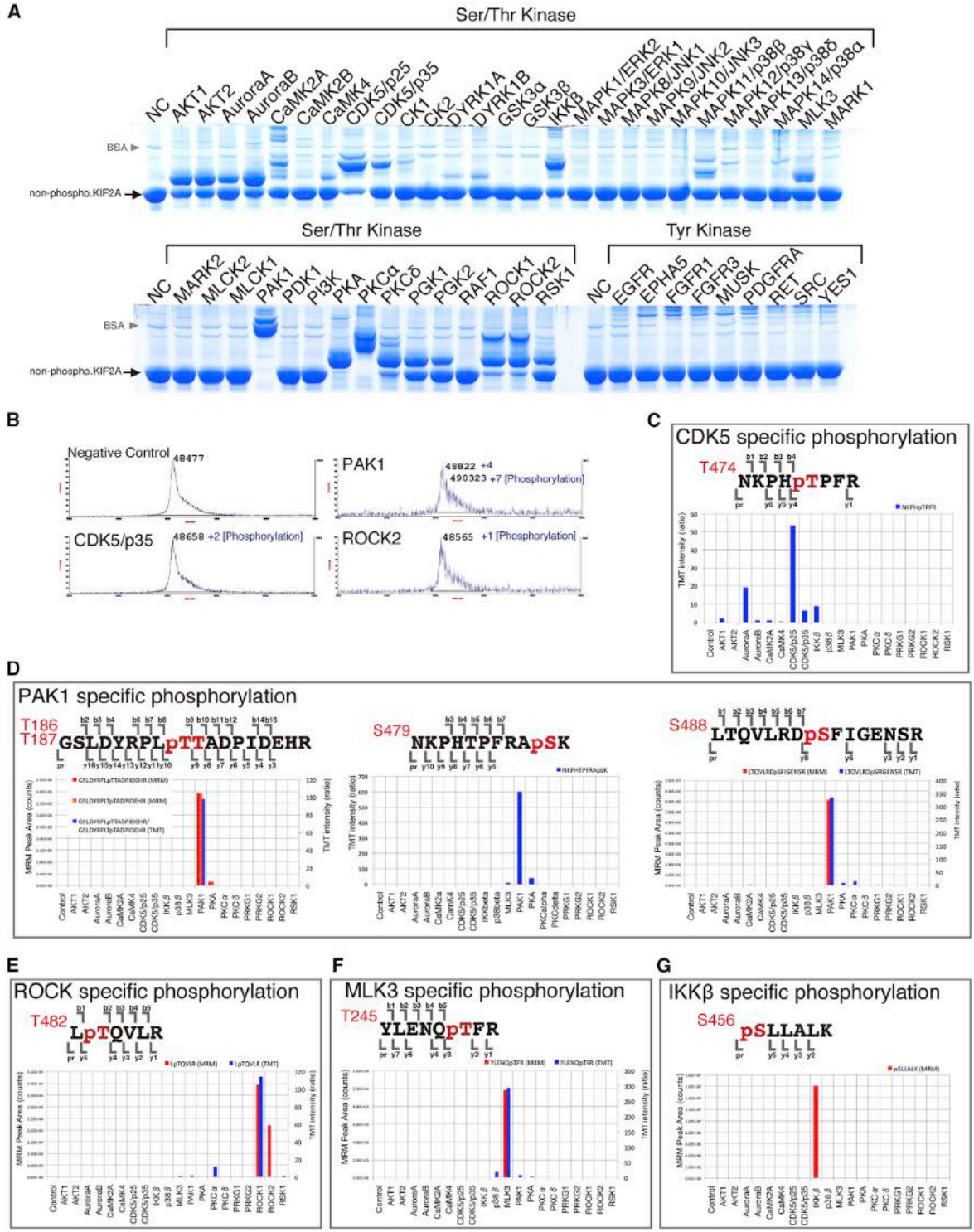

Figure 2. Specific Kinases Phosphorylate Specific Positions on KIF2A In Vitro

(A) KIF2Acore is phosphorylated by multiple kinases in vitro, as demonstrated by Phos-tag SDS-PAGE.

(B) Typical MALDI spectrum of KIF2Acore assayed without kinase (negative control) or with CDK5/p35, PAK1, or ROCK2. The peak spectra of the phosphorylated protein are shifted from those of the negative control at an *m/z* value of 80 (HPO_3^-). Δ (difference of the peak shift) = 80 × # (number of phosphorylation).

(C–G) Typical quantitation results are classified by the specific kinases. Each phospho-peptide was quantified by TMT (blue) and/or MRM (red/orange). Each phosphorylation site is presented as pS/pT in red.

See also Figures S3 and S4.

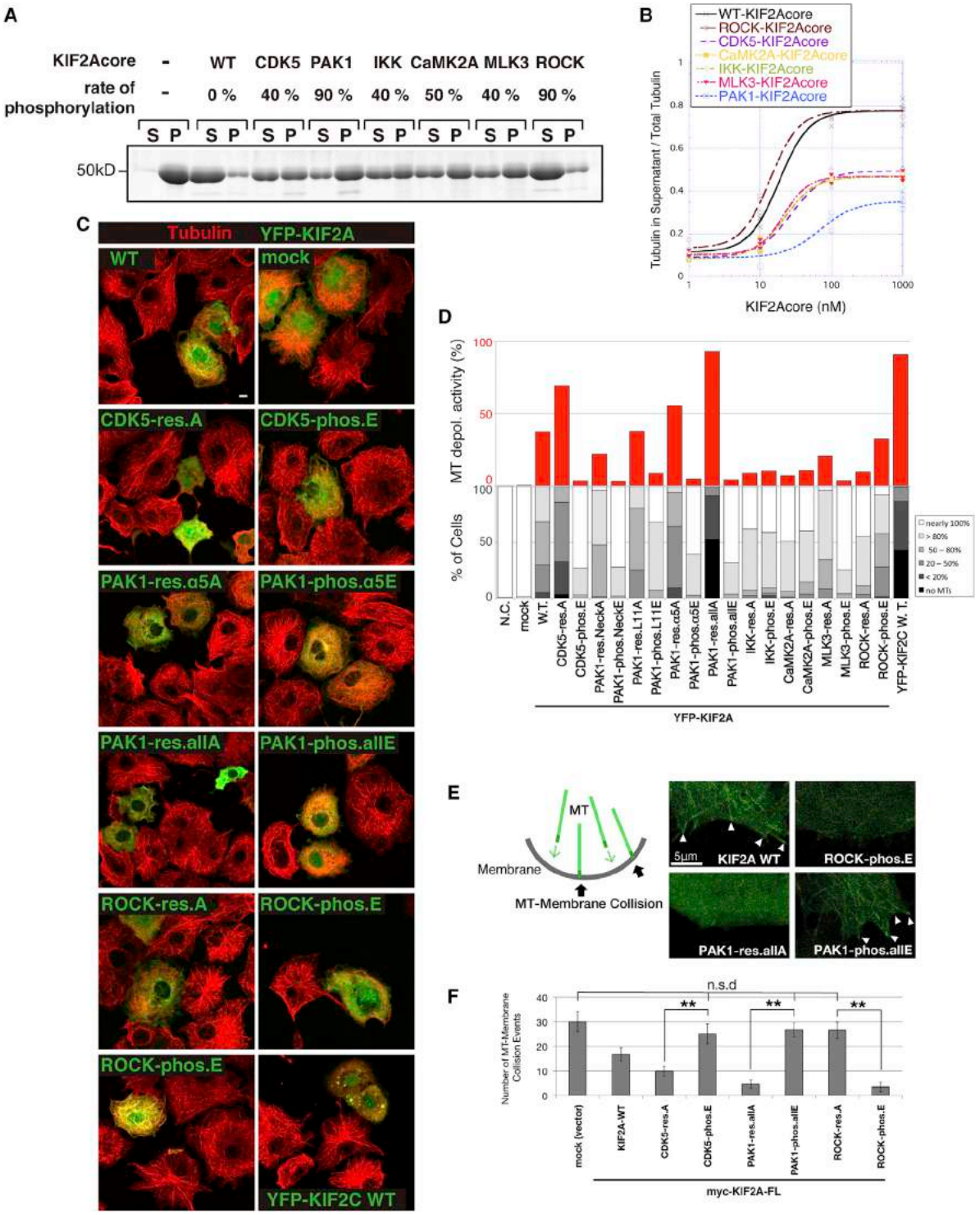

Figure 3. Site-Specific Phosphorylation of KIF2A Changes Its Microtubule Depolymerization Activity In Vitro and In Vivo

(A) MT depolymerization assay in vitro. Each phosphorylated KIF2Acore was incubated with GMPCPP-stabilized MTs in the presence of ATP followed by centrifugation. Equal volumes of the supernatant (S) and pellet (P) represent depolymerized tubulin and polymerized MTs, respectively. The phosphorylation rate of KIF2Acore is shown dependent on the each kinase.

(B) The ratio of tubulin in the supernatant to the total tubulin was fit to the sigmoidal dose-response curve.

(C) Fluorescent micrographs of EYFP-fused KIF2 FL mutants (green) and MTs (red) in COS-7 cells. Scale bar, 10 μm.

(legend continued on next page)

depolymerization was significantly accelerated; thus, no remaining MTs were observed. The activity was estimated to be approximately three times higher than that of WT KIF2A and equivalent to that of WT KIF2C. In the case of the three PAK1 phospho-mimetic KIF2A mutants, PAK1-phos.NeckE, PAK1-phos.L11E, and PAK1-phos.α5E, the MT depolymerization activity was almost abolished. PAK1-phos.allE also completely lost the MT depolymerization activity (Figures 3C and 3D).

The ROCK-resistant KIF2A T482A mutant (ROCK-res.A) showed activity that was lower than the WT KIF2A. In contrast, the ROCK phospho-mimetic KIF2A T482E mutant (ROCK-phos.E) produced complicated phenomena in which 80% of the transfected cells showed a diffuse distribution of ROCK-phos.E and the same MT depolymerizing activity as WT-KIF2A (Figures 3C and 3D). However, in 20% of the cells, ROCK-phos.E was tightly bound to the MTs. Interestingly, MTs decorated with ROCK-phos.E formed thick filaments at the cell periphery (Figure 3C). These results indicate that the MT depolymerization activity of ROCK-phos.E was highly dependent on its distribution in the cell; thus, some populations of ROCK-phos.E also functioned to form thick MTs in addition to their conventional MT depolymerization activity.

MLK3-resistant KIF2A (MLK3-res.A) showed a diffusive distribution and displayed MT depolymerizing activity. However, the MLK3 phospho-mimetic KIF2A (MLK3-phos.E) did not depolymerize MTs (Figure 3D); instead, MLK3-phos.E was bound to the MTs. Other mutants, including IKK-res.A, IKK-phos.E, CaMK2A-res.A, and CaMK2A-phos.E, showed decreased MT depolymerizing activity, although no significant difference was observed between the resistant and phospho-mimetic mutants (Figure 3D). This finding can be explained by the fact that the structural effects of the mutations were found to be stronger than the negative charge effect of the phospho-mimetic residues. Taken together, it can be concluded that the phosphorylated residues play a pivotal role in the MT depolymerizing activity of KIF2A; therefore, the upstream kinases CDK5, PAK1, and ROCK may regulate MT depolymerization via KIF2A phosphorylation.

To validate the direct effect of specific KIF2A phosphorylation sites on MT dynamics, the MT dynamics were observed in living COS-7 cells expressing EGFP-EB3 and Myc-tagged KIF2A FL phospho mutants, and the number of MT-membrane collision events was counted (Figures 3E and 3F). Consistent with the result of the MT depolymerization assay in fixed COS-7 cells, the Myc-tagged CDK5-res.A, PAK1-res.allA, and ROCK-phos.E KIF2A-FL mutants caused a small number of MT-membrane collision events, indicating their strong MT depolymerizing activities. In contrast, the CDK5-phos.E, PAK1-phos.allE, and ROCK-res.A mutants displayed similarly growing MTs as the control (Figures 3E and 3F; Movie S1). Both in vitro and in vivo observations suggest that specific kinases directly affect the MT depolymerizing activity of KIF2A via site-specific phosphorylation.

BDNF Evokes B-type Phosphorylation of KIF2A within Extending and Branching Neurons

The next question addressed was whether the kinase-specific phosphorylation of KIF2A occurs endogenously in neurons. Thus, primary neurons were exposed to extracellular stimuli, such as growth factors and lipid mediators. We first focused on brain-derived neurotrophic factor (BDNF), which is considered to be upstream of CDK5 and PAK1 (Figure 4A). CDK5 and PAK1 are required for BDNF-induced neurite growth (Cheung et al., 2007; Nikolic et al., 1996). However, the mechanisms that regulate MT dynamics after BDNF signaling still remain unclear. In addition, *Kif2a*$^{-/-}$ neurons show extended branches (Homma et al., 2003). Thus, we hypothesize that KIF2A is regulated by signaling downstream of BDNF to control MT dynamics in neurons.

To investigate the response of KIF2A phosphorylation, BDNF-stimulated cortical neurons were analyzed with the kinase inhibitors, RP106 (for CDK5) and IPA-3 (for PAK1). Phos-tag WB showed that KIF2A phosphorylation was induced after BDNF stimulation and was suppressed by kinase inhibitors (Figure 4B). BDNF induced WT neurons with 60% more branches and 40% longer processes compared to the negative control, which were similar to *Kif2a*$^{-/-}$ neurons. Interestingly, these morphological effects were suppressed by the inhibitors only in WT neurons; in contrast, there were few effects in *Kif2a*$^{-/-}$ background neurons (Figures 4C and 4D). These observations suggest that KIF2A and PAK1/CDK5 function in the same signaling pathway in BDNF-stimulated neurons with extending and branching processes.

To quantify the site-specific phosphorylation of endogenous KIF2A, the phospho-peptides from stimulated neurons were analyzed by MRM. As a result, BDNF induced increases in PAK1-dependent phosphorylation of T186/T187, S479, and S488, as well as in CDK5-dependent phosphorylation of T474 (Figures 4E, S6A, and S6B). Remarkably, T474 and S479 phosphorylation were significantly increased (Figure 4E). These results confirmed that the PAK1/CDK5-specific phosphorylation of KIF2A predominantly occurs in neurons in response to BDNF stimulation.

LPA Enhances ROCK Activity to Direct A-type KIF2A Phosphorylation

Next, we investigated the effect of ROCK signaling on KIF2A phosphorylation. Lysophosphatidic acid (LPA) is a potent lipid mediator that stimulates the Rho/ROCK signaling cascade via

(D) The relative MT depolymerizing activity of the various KIF2 mutants. The cells were classified by the number of remaining MTs into six categories: no MTs (black in the lower panel), <20% (dark gray), 20%–50% (gray), 50%–80% (light gray), >80% (faint gray), and nearly 100% (white), and the number of cells in each category was counted (lower panel). The mean degree of MT depolymerization was calculated from this scoring and plotted as the relative MT depolymerizing activity (upper panel).

(E) Live imaging analysis of the dynamic plus end of MTs using EGFP-EB3 (green) in COS-7 cells expressing the Myc-tagged KIF2A FL phospho mutants. Scale bar, 5 μm. See also Movie S1.

(F) The collision events (arrowheads in E) between dynamic MTs and the plasma membrane in a 20-μm width were counted for 5 min. Mean ± SD; n.s.d. (no significant difference) > 0.01; *p < 0.01, and **p < 0.001 using Student's t test; n = 10 cells from three independent experiments.

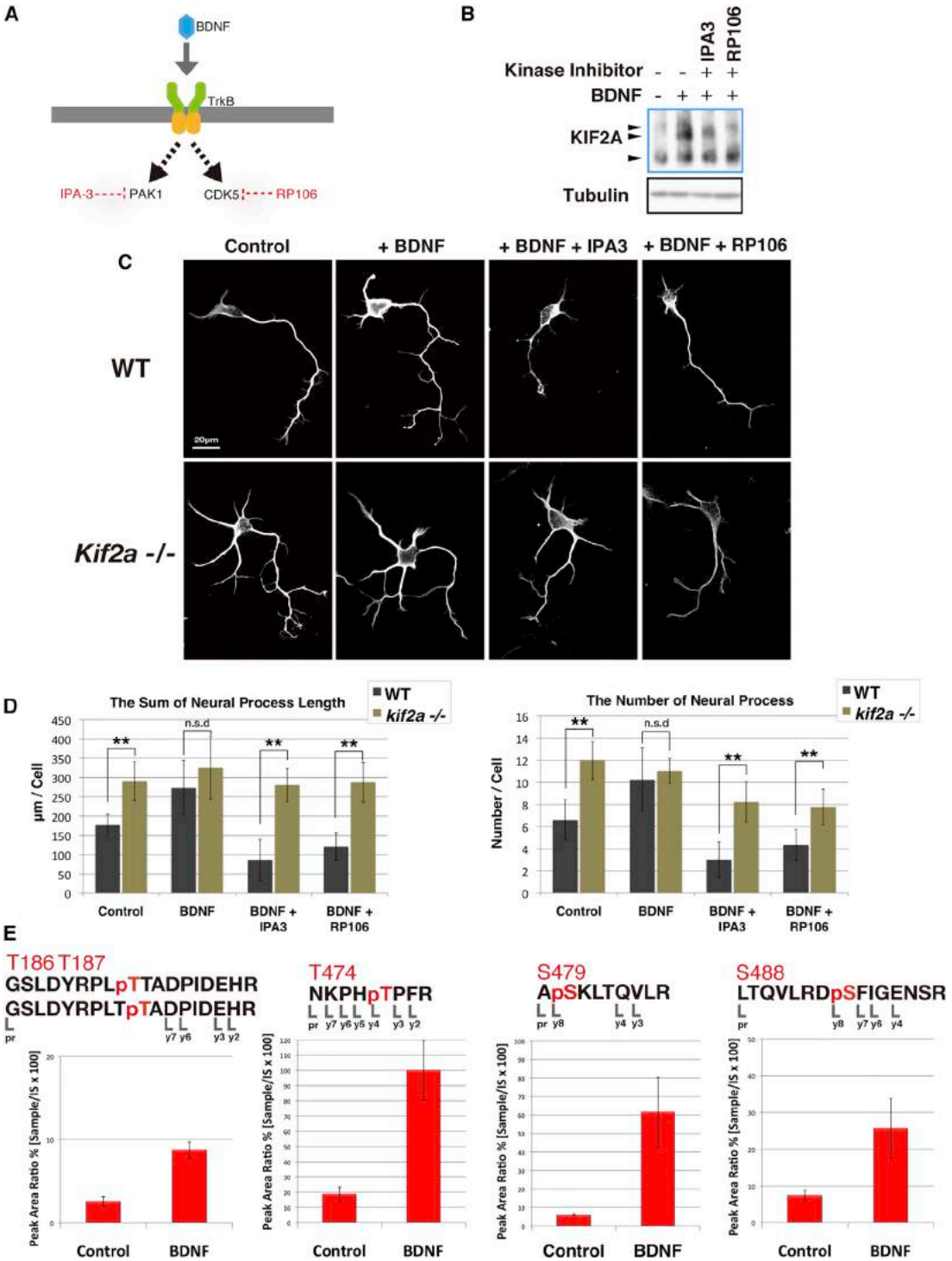

Figure 4. Neuronal Phenotype and Site-Specific Quantitative Analysis of KIF2A Phosphorylation after BDNF Stimulation

(A) BDNF signaling cascade based on information from the literature.

(B) The total KIF2A phosphorylation after BDNF stimulation was analyzed using Phos-tag WB (blue box). Tubulin was used as a loading control in conventional WB (black box).

(C) BDNF-stimulated cortical neurons (WT or *Kif2a*$^{-/-}$) with or without inhibitors. Tubulin (white: DM1A) was stained to visualize the overall morphology. Scale bars, 20 μm.

(legend continued on next page)

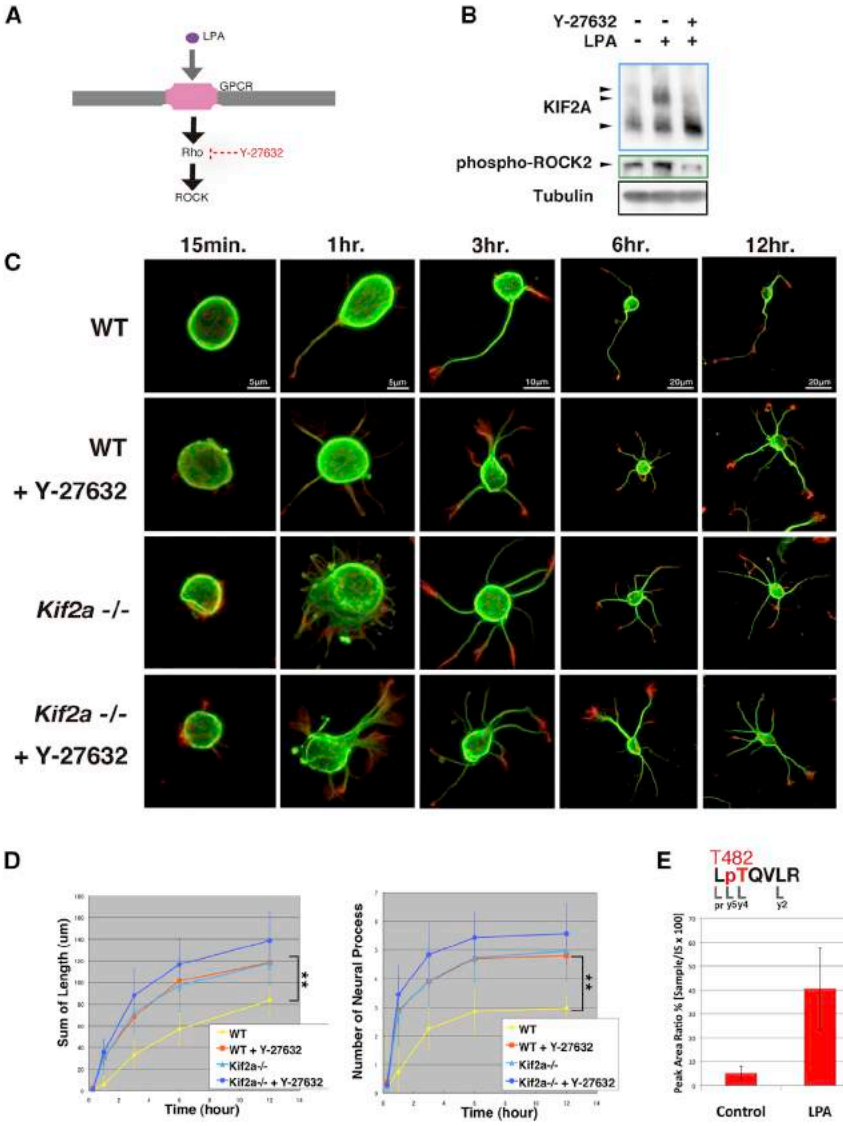

Figure 5. Neuronal Phenotype and Site-Specific Quantitative Analysis of KIF2A Phosphorylation with Stimulation or Inhibition of ROCK Signaling

(A) Rho-ROCK signaling occurs downstream of the LPA receptor, a GPCR; it is inhibited by Y-27632.

(B) Total KIF2A phosphorylation was observed using Phos-tag WB (blue box) and activated ROCK2 was observed with conventional WB (green box) after stimulation and inhibition of ROCK signaling. Tubulin was used as a loading control in conventional WB (black box).

(C) Y-27632 accelerated neurite outgrowth in wild-type neurons. *Kif2a*$^{-/-}$ neurons showed outgrowth of multiple neurites regardless of the presence or absence of Y-27632. Tubulin (green: DM1A) and actin (red: phalloidin) were visualized. Scale bars represent 5 μm in 15 min and 1 hr, 10 μm in 3 hr, and 20 μm in 6 hr and 12 hr.

(D) The sum of the neurite lengths and the numbers of neurites were counted per cell. Mean ± SD; n.s.d. > 0.01, *p < 0.01, **p < 0.001 using Student's t test; n = 50 neurons from three independent experiments.

(E) There was a significant increase in T482 phosphorylation in LPA-stimulated round neurons. The peak area ratios are the ratios of the peak area of the fragmented ions of each sample to that of the internal standard (IS). Each data point represents the mean ± SEM of data collected from four MRM transitions.

See also Figures S2 and S6 and Tables S3 and S4.

its specific G-protein-coupled receptor (GPCR) (Figure 5A). In neurons, LPA induces neurite shortening, enhances cell rounding, and prevents neurite outgrowth (Riento and Ridley, 2003). When Rho/ROCK signaling is blocked by the selective ROCK inhibitor Y-27632, neurite outgrowth is initiated from round cells (Bito et al., 2000). Based on the results that ROCK phosphorylated T482 on KIF2A in vitro (Figure 2E) and the fact that the branched *Kif2a*$^{-/-}$ neurons (Figure 4C) exhibited the opposite phenotype of ROCK-activated neurons, we hypothesized that KIF2A is in the ROCK signaling pathway during neuronal morphogenesis.

To examine the effect of ROCK on KIF2A phosphorylation, cortical neurons were exposed to LPA and Y-27632 at 1 day in vitro (DIV). Phos-tag WB displayed rapid increases in active ROCK2 and KIF2A phosphorylation after LPA stimulation; in contrast, these were clearly blocked by Y-27632 (Figure 5B). We next focused on the LPA-induced ROCK-mediated neuronal phenotypes of neurite retraction and cell rounding. No significant difference was observed in LPA-stimulated neurite retraction between the WT and *Kif2a*$^{-/-}$ neurons (Figure S6). When primary neurons are plated, the cells are rounded (Figure 5C). As reported previously, ROCK inhibition with Y-27632 initiated rapid neurite outgrowth from round WT neurons. Strikingly, Y-27632 did not affect neurite outgrowth from *Kif2a*$^{-/-}$ neurons (Figures 5C and 5D), suggesting that KIF2A and ROCK signaling are involved in the same pathway. Furthermore, the site-specific phospho-analysis using MRM displayed a significant increase in T482 phosphorylation upon LPA stimulation (Figures 5E, S6D, and S6E),

(D) The sum of the neural process length and the number of neural processes per cell. Mean ± SD; n.s.d. (no significant difference) > 0.01, *p < 0.01, **p < 0.001 using Student's t test; n = 30 from three independent experiments.

(E) BDNF stimulation produced a significant increase in site-specific KIF2A phosphorylation. The peak area ratios are the ratios of the peak area of the fragmented ions from each sample to that of the internal standard (IS). Each data point represents the mean ± SEM of data collected from at least four MRM transitions.

See also Figure S2 and Tables S1 and S2.

indicating that KIF2A phosphorylation by ROCK may be a key pathway for suppressing neurite outgrowth from the round cells.

Non-phosphorylatable KIF2A Mutants Suppress the Cellular Effects of A- and B-type Signal Transduction

As described above, KIF2A was selectively phosphorylated in specific signaling cascades; however, it remains unclear whether these phosphorylations are critical events for the phenotype or simply byproducts in neurons. To address this question, we analyzed the phenotypes of stimulated *Kif2a*$^{-/-}$ neurons expressing the kinase-specific KIF2A mutants.

First, we investigated whether PAK1/CDK5-dependent KIF2A phosphorylation is critical for the BDNF-induced neuronal phenotype (Figures 6A and 6B). As a control, YFP-KIF2A (WT) strongly rescued the branching phenotype of the *Kif2a*$^{-/-}$ neuron, while this rescue activity was suppressed by BDNF stimulation. However, the PAK1/CDK5-resistant KIF2A mutants displayed the opposite phenotype, shorter and fewer neural processes, even under BDNF stimulation (Figures 6A and 6B). Among the resistant mutants, PAK1-res.allA showed the most significantly shifted phenotype. These results indicate that the PAK1/CDK5-specific phosphorylation of KIF2A is crucial for the outgrowth of neural processes under BDNF stimulation. Together with the previous results (Figures 3 and 4), these findings suggest that BDNF downregulates the MT depolymerizing activity of KIF2A through PAK1/CDK5-specific phosphorylation of KIF2-specific clusters, resulting in the outgrowth of neural processes.

Next, we tested whether ROCK-specific KIF2A phosphorylation is crucial for the suppression of neurite outgrowth from round cells. Interestingly, the initiation of neurite outgrowth by ROCK inhibition with Y-27632 was only observed in *Kif2a*$^{-/-}$ neurons expressing YFP-KIF2A (WT). The ROCK-phos.E mutant displayed fewer and shorter neuritis, regardless of the presence or absence of Y-27632 (Figures 6C and 6D). These results indicate that the ROCK-specific T482 phosphorylation of KIF2A is a critical event that occurs downstream of ROCK signaling to suppress neurite outgrowth from round cells.

To validate the effect of the specific phosphorylation events on MT dynamics, the growing MTs were observed using EGFP-EB3 and Myc-tagged KIF2A FL phospho mutants in living *Kif2a*$^{-/-}$ neurons. The CDK5-res.A, PAK1-res.allA, and ROCK-phos.E mutants caused a small number of MT-membrane collision events (Figures 6E and 6F; Movie S2), indicating that PAK1/CDK5-resistant KIF2A and ROCK phospho-KIF2A function as MT suppressers. In contrast, the CDK5-phos.E, PAK1-phos.allE, and ROCK-res.A mutants did not change the MT dynamics in the *Kif2a*$^{-/-}$ neurons (Figures 6E and 6F; Movie S2). These observations confirmed that specific phosphorylation events directly change the MT depolymerizing activity of KIF2A, resulting in neuronal morphological changes.

B-type Phosphorylation Impairs the Tubulin-Stimulated ATPase Activity and the Association of KIF2A with Tubulin

The next question to be considered is how these phosphorylation events regulate the MT depolymerizing activity of KIF2A. MT depolymerization by KIF2 is reported to be composed of two mechanical KIF2-specific activities. One activity is for KIF2 to form a nucleotide-sensitive complex with the tubulin dimer (Desai et al., 1999; Hertzer et al., 2006; Moores et al., 2002). The other critical activity is tubulin-stimulated ATPase activity (Hertzer et al., 2006; Hunter et al., 2003; Moore and Wordeman, 2004). In addition, we presented that the phosphorylation sites were positioned within KIF2-specific clusters (Figures 1A and 7A): the "neck," "KDV-finger" (loop2), "switch I" (alpha2-Loop9), and "switch II" (alpha4-alpha6), which are important for these KIF2-specific activities (Ogawa et al., 2004). Therefore, we focused on these two critical activities to dissect the effects of KIF2 phosphorylation.

Each phosphorylated KIF2Acore protein was incubated with tubulin in the presence of ATP, and the released ADP was directly measured by anion exchange chromatography (Figure 7B, boxed panel). Compared to the unphosphorylated WT-KIF2Acore, PAK1-KIF2Acore displayed a 10-fold reduction in ATPase activity. CDK5-KIF2Acore also showed a dramatic decrease in spite of its low phosphorylation rate (40%). In contrast, ROCK-KIF2Acore did not significantly reduce its ATPase activity, in spite of its high phosphorylation rate (90%) (Figure 7B). In the KIF2-tubulin binding assays, PAK1-KIF2Acore showed a 2-fold reduction in the affinity with tubulin (K_d 4.57) compared to WT-KIF2Acore (K_d 2.67), while ROCK-KIF2Acore showed the same or higher affinity as WT-KIF2Acore (Figure 7C). These results indicate that PAK1 and CDK5 directly reduce both the tubulin-stimulated ATPase activity and the KIF2A association with the tubulin dimer via specific phosphorylation events, resulting in the loss of MT depolymerization activity.

DISCUSSION

In this study, we demonstrated that there is a well-organized mechanism regulating MT dynamics via distinct site-specific phosphorylation of KIF2A in neurons in response to extracellular signals. We generated the complete phosphorylation map of KIF2A and identified the specific kinases for each site. We further found that CDK5 and PAK1 decrease the MT depolymerizing activity of KIF2A through site-specific phosphorylation, resulting in enhanced outgrowth of neural processes. In contrast, ROCK2 suppresses neurite outgrowth from round cells via ROCK-specific KIF2A phosphorylation.

Therefore, we propose a model for the mechanism of controlling KIF2A activity to regulate MT dynamics in stimulated neurons (Figure 7D). In round neurons, KIF2A is phosphorylated at T482 by ROCK2. This phosphorylation transforms un-regulated KIF2A into "A-KIF2," whose MT depolymerization activity is "accelerated" and maintained in an "active" state. This cascade contributes to maintain cell rounding. Once blocked by Y-27632, neurite outgrowth occurs along with MT growth. In BDNF-stimulated neurons, the MT depolymerization activity of KIF2A is "braked" as "B-KIF2" by PAK1-/CDK5-specific phosphorylation, resulting in the outgrowth of neural processes. Our model reflects the details of the multiple distinct phosphorylation cascades for KIF2A to regulate MT dynamics as A-KIF2 after ROCK signaling or B-KIF2 after BDNF signaling (Figure 7D).

Most phosphorylation sites were positioned within KIF2-family-specific structural clusters (Figures 1A and 7A). The kinases recognize specific motifs and specific structures. It

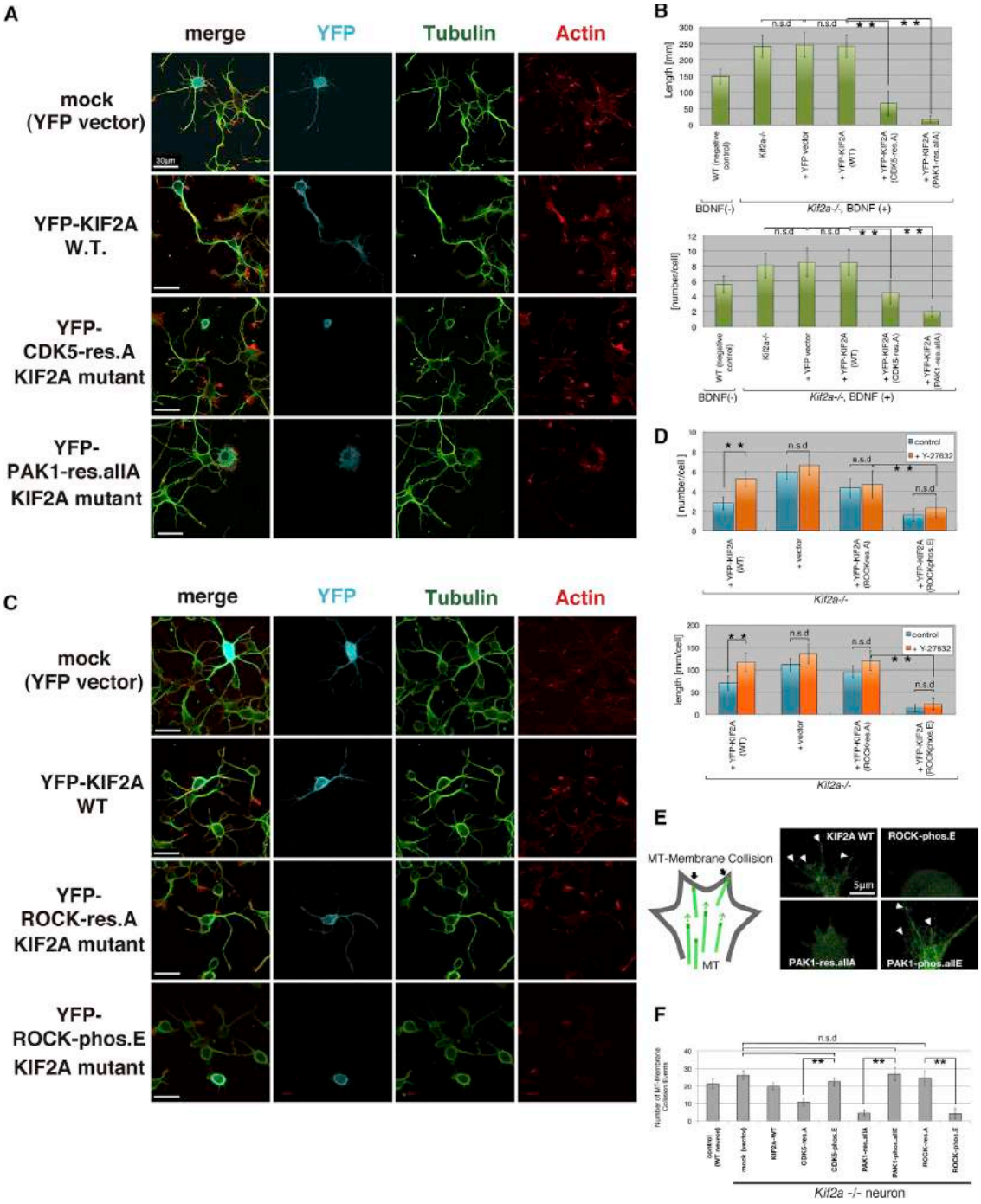

Figure 6. Phosphorylation-Resistant Mutations Reverse the Neuronal Phenotype under Stimulation

(A) The kinase-resistant KIF2A mutants (turquoise blue), tubulin (green), and actin (red: phalloidin) in BDNF-stimulated *Kif2a*$^{-/-}$ neurons.

(B) The sum of the neural process lengths and the number of neural processes under BDNF stimulation were counted for each cell.

(C) ROCK-specific KIF2A mutants (turquoise blue), tubulin (green), and actin (red: phalloidin) in *Kif2a*$^{-/-}$ cortical neurons treated with Y-27632.

(D) The sum of the neurite length and the number of neurites were counted for each cell with or without Y-27632 treatment.

(E) Live imaging analysis of the dynamic plus end of MTs using EGFP-EB3 (green) in *Kif2a*$^{-/-}$ dissociated cortical neurons expressing the Myc-tagged KIF2A FL phospho mutants. Scale bars, 5 μm. See also Movie S2.

(F) The collision events (arrowheads in E) between dynamic MTs and plasma membrane in a 20-μm width were counted for 5 min.

All values are shown as the mean ± SD; n.s.d. > 0.01; *p < 0.01, and **p < 0.001 were considered statistically significant. Student's t test; n = 30 (A–D) or 10 (E and F) from three independent experiments.

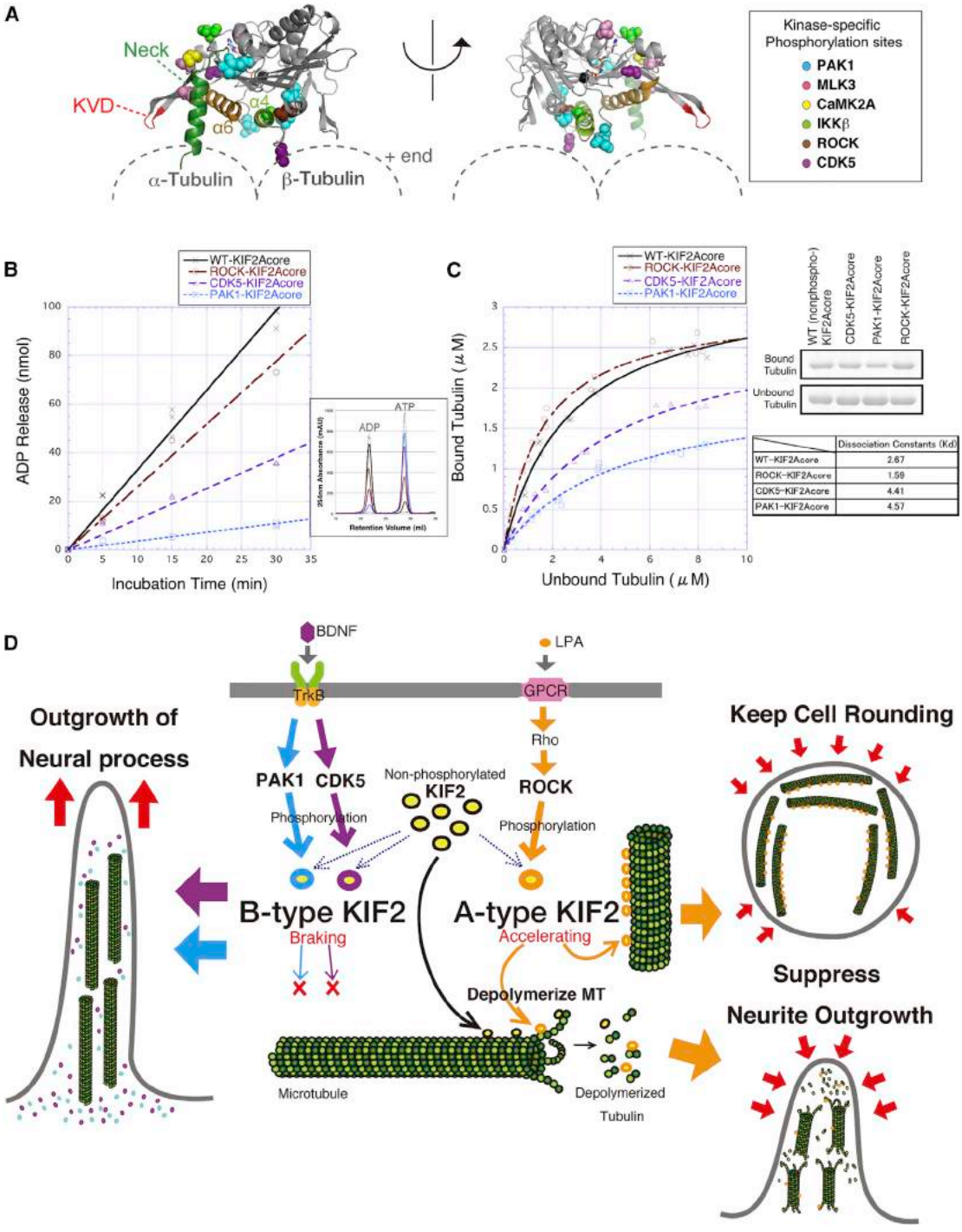

Figure 7. Mechanism and Model of MT Regulation via KIF2A Phosphorylation

(A) Positions of kinase-specific phosphorylation sites on a 3D structure of KIF2core-tubulin. CDK5 phosphorylates the switch II cluster. PAK1 targets the neck and switch II. ROCK is responsible for alpha5 phosphorylation in switch II. MLK3, IKKβ, and CaMK2A preferentially phosphorylated residues around the KVD finger. The model is modified from the crystal structure of KIF2Ccore (PDB: 1V8K) using PyMOL.

(B) Tubulin-stimulated ATPase activity of phosphorylated KIF2Acore. The amount of ADP released from ATP hydrolysis was directly measured on high-performance liquid chromatography (boxed panel).

(C) KIF2-tubulin binding assay. The amount of bound/unbound tubulin to KIF2 was plotted and analyzed by hyperbolic equation to calculate K_d.

(D) Model: KIF2A undergoes multiple distinct phosphorylation cascade to regulate MT dynamics as "A-type KIF2" under ROCK signaling or "B-type KIF2" under BDNF signaling.

See also Figure S7.

is reasonable that specific kinases distinguish KIF2-specific clusters from the many other KIFs that swarm in the cell. In addition to the kinase specificity, the spatial and temporal coexistence of activated kinases and the substrate distribution are also key factors in the generation of a proper response. We analyzed the intracellular distribution of activated kinases and KIF2A in stimulated neurons using anti-phospho-kinase (CDK5, PAK1, and ROCK2) and anti-KIF2A antibodies. In BDNF-stimulated neurons, active PAK1/CDK5 and KIF2A were diffusely co-expressed in the shafts of neural processes (Figures S7A and S7B). In LPA-stimulated neurons, active ROCK2 and KIF2A were well colocalized at the periphery of the cell body (Figure S7C). These distributions indicate that each activated kinase temporally co-exists with KIF2A in response to the stimuli.

PAK1 has been reported to phosphorylate stathmin/Op18, another MT destabilizer, blocking its MT destabilization activity (Daub et al., 2001). It is rational that KIF2A and stathmin/Op18 are involved in the same signaling pathway to regulate MTs. CDK5 is reported to be a key regulator of neurodegeneration. In healthy contexts, p35/CDK5 regulates MT dynamics. In contrast, p25/CDK5 hyper-phosphorylates the MT-associated proteins Tau and MAPs in neurodegenerative diseases (Patrick et al., 1999). In fact, T474 in KIF2A is hyperphosphorylated by p25/CDK5; in contrast, S503 is phosphorylated by p35/CDK5 in vitro (Figures 2A, 2C, and S3B). We speculate that the different balance of these phosphorylation events underlies between the healthy and disease contexts. Further investigations using in vivo disease models to examine the phosphorylation of KIF2A in neurodegenerative diseases may be particularly interesting.

The LPA-induced Rho/ROCK pathway is also reported to involve PIP5K (van Horck et al., 2002). Recently, our group reported that PIP5K interacts with KIF2A to suppress the elongation of axon branches (Noda et al., 2012). Therefore, it is rational that KIF2A is involved in Rho/ROCK signaling and directly phosphorylated by ROCK to regulate MT dynamics in neurons.

The Different MT Depolymerizing Activities of KIF2A and KIF2C/MCAK May Be Explained by Changes in the Phosphorylatable Residues

KIF2A showed MT depolymerization activity that was approximately one-third of that of KIF2C in cells (Ogawa et al., 2004) (Figures 3C and 3D). The mechanism of how this different activity in cells is manifested has been unknown, despite their high amino acid sequence identity (86%, KIF2Acore versus KIF2Ccore). In this study, the PAK1-resistant mutations overcame the low MT depolymerization activity of KIF2A to produce the same activity as KIF2C (Figures 3C and 3D) in cells. However, KIF2Acore displayed strong MT depolymerizing activity in vitro (Figures 3A and 3B), and the activity was similar to that of KIF2Ccore (MD-MCAK, *Xenopus* MCAK aa 187–592) in a previous report (Hertzer et al., 2006). Together, this circumstantial evidence shows that PAK-specific phosphorylation may underlie the difference. Moreover, KIF2A and KIF2C have different sensitivities to kinases in vivo. In fact, T187, a PAK target, is only conserved in KIF2A and is replaced with hydrophobic residues in KIF2C. In addition, T245 of KIF2A, an MLK3 target, is also replaced with alanine in the KIF2C subfamily. These amino acid substitutions may help KIF2C to maintain its strong activity against the inhibitory effects of the kinases. Because KIF2A is ubiquitous in cells, including neurons, whereas KIF2C mainly functions in mitotic cells, it is plausible that the differential sensitivity produces the proper activity for each context.

Crosstalk between MTs and Other Cytoskeletal Components in Neurons

To date, rapid changes in neurite outgrowth have been explained by the modulation of actin dynamics through key regulators such as the Rho GTPases RhoA, Rac1, and Cdc42. Under BDNF stimulation, Cdc42 is reported to activate PAK1 to induce actin polymerization through LIMK-Cofilin signaling (Cau and Hall, 2005). Cdc42/Rac1 signals are also transferred through the WASP-WAVE-ARP2/3 protein network to promote actin polymerization (Takenawa and Miki, 2001). CDK5 is reported to be activated after BDNF signaling to induce neurite outgrowth (Cheung et al., 2007; Nikolic et al., 1996). However, the BDNF-induced pathways leading to MT polymerization have been poorly understood. Some papers have suggested the link between the PAK1/CDK5 signals and MT polymerization (Daub et al., 2001; Patrick et al., 1999). In the current study, we reveal that CDK5 and PAK1 directly control the MT dynamics via KIF2A phosphorylation.

The neurite retraction following ROCK activation and the neurite outgrowth following ROCK inhibition (Bito et al., 2000) (Figure 5C) have been mainly explained by the regulation of the actin network (Riento and Ridley, 2003); however, some reports suggested that ROCK inhibition induces the MT bundles that accompany the enlargement in growth cones (Bito et al., 2000). We demonstrated that *Kif2a*$^{-/-}$ neurons displayed a significant defect in suppression of neurite outgrowth from the round neurons (Figures 5C and 5D), but not in the neurite retraction phenotype (Figure S6). We speculate that MTs predominate over actin in the initiation of neurite outgrowth; however, actin produces the driving force in neurite retraction.

We observed a strong reversal of the phenotype in neurons with kinase-specific KIF2A mutations (Figure 6). In these neurons, actin dynamics may also be regulated. To date, there have been no reports that KIF2 directly affects actin dynamics. Thus, this strong phenotype is explained by the feedback effects from the substrate to the upper cascade or by indirect connections between MTs and actin. Taken together, the regulation of MTs and the actin cytoskeleton may be controlled through the same signaling cascade in certain cases and by independent cascades under other circumstances.

Future Directions

We have directly demonstrated that ROCK acts as an "accelerating" kinase; in contrast, CDK5 and PAK1 act as "braking" kinases for KIF2A activity. Interestingly, these functionally opposed phosphorylation sites are located in close proximity (Figure 1A). Thus, the phosphorylation must be exquisitely tuned and balanced even in complex in vivo systems. In this work, we focused on PAK1/CDK5/ROCK-dependent KIF2A phosphorylation in primary cortical neurons at early developmental stages. However, other kinases and complex systems may be involved in other contexts. Other candidate kinases, such as AKT, MLK3, CaMK2A, IKKβ, and PKCα, will require optimized in vivo systems at the tissue or individual level.

The molecular mechanisms of how phosphorylation controls the MT depolymerizing activity of KIF2 should also be investigated further. We demonstrated that phosphorylation affects the ATPase activity and the affinity between KIF2 and the tubulin dimer (Figures 7B and 7C). In addition, some reports suggested that the C-terminal region contributes to the activity and regulation of KIF2 (Hertzer and Walczak, 2008; Hertzer et al., 2006; Moore and Wordeman, 2004). Therefore, other domains and additional factors also should be considered in further analyses. Precise structural analyses will reveal the critical conformations that are driven by specific phosphorylation.

To identify the key molecules and provide a broad and in-depth understanding of the target phenomena, it is crucial to discover the molecules of interest, identify the dynamic changes in the target molecules, and quantify their behavior under diverse conditions. Here, we have used systematic approaches to transform the conventional qualitative analysis into systematic, quantitative, and targeted analyses. Thus, our strategic approaches are promising for understanding target molecules and their phenotypes from quantitative perspectives.

EXPERIMENTAL PROCEDURES

KIF2A Constructs

FL mouse *Kif2a* was mutated to generate the following kinase-resistant or phospho-mimetic constructs: T474A/S503A (CDK5-res.A), T474E/S503E (CDK5-phos.E), T186A/T187A (PAK1-res.NeckA), T186E/T187E (PAK1-phos.NeckE), T439A/S440A/S441A (PAK1-res.L11A), T439E/S440E/S441E (PAK1-phos.L11E), S479A/S488A (PAK1-res.α5A), S479E/S488E (PAK1-phos.α5E), T186A/T187A/T439A/S440A/S441A/S479A/S488A (PAK1-res.allA), T186E/T187E/T439E/S440E/S441E/S479E/S488E (PAK1-phos.allE), T482A (ROCK-res.A), T482E (ROCK-phos.E), S255A/S456A (IKK-res.A), S255E/S456E (IKK-phos.E), S222A (CaMK2A-res.A), S222E (CaMK2A-phos.E), T219A/T245A/S300A (MLK3-res.A), and T219E/T245E/S300E (MLK3-phos.E) (summarized in Figure S5). The EYFP-fusion FL fusion constructs and KIF2Acore protein were prepared as previously described (Ogawa et al., 2004).

In Vitro Kinase Assay and Phosphorylated KIF2Acore Proteins

The bacterially expressed KIF2Acore protein was assayed with active kinases at 30°C for 60 min. Each reaction was analyzed by Phos-tag SDS-PAGE and mass spectrometry. The purified phospho-KIF2Acore protein was used for biochemical assays, in which the glutathione S-transferase-tagged active kinase and ATP were depleted using glutathione Sepharose and size exclusion chromatography. The phosphorylation rate was estimated by Phos-Tag SDS-PAGE.

In Vitro MT Depolymerization Assay

GMPCPP-stabilized MTs (5 μM) were incubated with increasing concentrations of each purified phosph-KIF2Acore (0 nM to 1 μM) in BRB80K150 (80 mM PIPES, 150 mM KCl, and 1 mM $MgCl_2$) containing 1 mM ATP for 20 min at 27°C. The reactions were sedimented and processed for conventional SDS-PAGE analysis. The ratio of tubulin in the supernatant to the total tubulin from at least three independent experiments was analyzed by the sigmoidal dose-response curve using KaleidaGraph.

MT Depolymerization Assay in COS-7 Cells

COS-7 cells were transfected with the EYFP-fused FL KIF2A constructs and fixed 26 hr after transfection. The MT arrays were visualized using the anti-α-tubulin antibody DM1A (Sigma) and an Alexa Fluor 568-labeled secondary antibody (Molecular Probes). The fixed samples were observed with an inverted fluorescent microscope (Axio Observer.Z1, Zeiss) equipped with a spinning-disk confocal unit (CSU-W1, Yokogawa). The amount of plasmid DNA and the transfection conditions were adjusted to achieve a consistent transfection efficiency and similar expression levels of the EYFP signal. For each construct, 300 transfected cells were randomly chosen, and the degree to which the MT array was lost in each cell was scored as previously described (Ogawa et al., 2004).

Live Imaging Analysis of Microtubule Dynamics in COS-7 Cells and Cortical Neurons

The COS-7 cells or *Kif2a*$^{-/-}$ dissociated cortical neurons were transfected with EGFP-EB3 and Myc-tagged KIF2A FL phospho mutants, WT-, CDK5-, PAK1-, and the ROCK-KIF2A kinase-resistant/phospho-mimetic mutants. Growing MTs were observed under an LSM 710 confocal microscope (Carl Zeiss). The collision events between dynamic MTs and plasma membrane in a 20-μm width were counted for 5 min in 10 cells from at least three independent experiments for each mutant. Student's t test was used to compare the data between the two groups.

Kinase Stimulation and Inhibition

The dissociated cortical neurons were stimulated with BDNF (50 ng/ml) with or without inhibitors at stage 3 (1 DIV) and fixed 12 hr later. CDK5 and PAK1 were blocked with RP106 (10 μM) and IPA-3 (10 μM), respectively. The cortical neurons were stimulated with LPA (1 μM) with or without the ROCK inhibitor Y-27632 (10 μM) at stage 3 (1 DIV) and fixed 15 min later.

MALDI-TOF/TOF Analysis

An ABI4700 MALDI-TOF mass spectrometer (AB SCIEX) was used to identify the proteins (MS/MS mode) and to analyze phospho-peptides and phospho-proteins (linear mode).

Qualitative Phospho-analysis In Vivo

Native KIF2A was immuno-precipitated from the E16 mouse brain (Figure S1A). After tandem affinity phospho-peptide enrichment, the digested peptides were analyzed by MALDI-TOF and LC-MSn using an LTQ or LTQ-Orbitrap Velos (Thermo Scientific). MS2 and MS3 fragments were used to assign the phosphorylation sites.

Site-Specific Quantitative Phospho-analysis In Vitro

The basic strategies of the site-specific quantitation are described in Figure S2. The TMT-labeled samples were analyzed via tandem mass spectrometry, using an LTQ-Orbitrap Velos. Quantitation was achieved by comparing the intensities of the unique reporter ions from TMT. Non-labeled samples were analyzed by MRM using a triple-quadrupole ion trap mass spectrometer 4000QTRAP (AB SCIEX) and TSQ Vantage (Thermo Scientific) with a Zaplous-NanoLC system (AMR) that was customized for phospho-peptides.

Site-Specific Quantitative Phospho-analysis In Vivo

The proteins extracted from four culture dishes of stimulated primary cortical neurons were digested into peptides. The bacterially expressed 15N-labeled KIF2Acore protein was phosphorylated by kinases in vitro, digested, and mixed into each in vivo sample as an internal standard (IS). Quantitative data were obtained using the 6500QTRAP triple-quadrupole ion trap mass spectrometer (AB SCIEX). Quantitation was achieved by calculating of the peak area ratio (endogenous peptide/IS).

ATPase Assay of Phosphorylated KIF2Acore

The amount of released ADP was directly measured to analyze ATPase activity. Phospho-KIF2Acore protein (10 nM) and tubulin dimers (20 nM) were incubated in BRB20K200 (20 mM PIPES, 200 mM KCl, and 1 mM $MgCl_2$) with 100 nM ATP for 5, 15, and 30 min. ADP was separated by anion exchange chromatography on AKTA system (GE) and quantified from the peak area of each chromatogram.

KIF2/Tubulin Dimer Binding Assay

The phosphorylated KIF2Acore protein (3 μM) was incubated with 0–12 μM tubulin in BRB80K150 containing 1 mM AMP-PNP (Roche) for 20 min at room temperature. The KIF2Acore protein and bound tubulin were captured by Ni resin (Clontech). Bound and unbound tubulin was analyzed using

SDS-PAGE and ImageJ. To calculate the K_d, the bound tubulin dimer versus unbound tubulin was analyzed by nonlinear regression in KaleidaGraph by using the hyperbolic equation.

A full version of the experimental procedures is provided in Supplemental Experimental Procedures.

SUPPLEMENTAL INFORMATION

Supplemental Information includes Supplemental Experimental Procedures, seven figures, four tables, and two movies and can be found with this article online at http://dx.doi.org/10.1016/j.celrep.2015.08.018.

AUTHOR CONTRIBUTIONS

T.O. and N.H. conceived the project. T.O. performed the experiments, and T.O. and N.H. analyzed the data. T.O and N.H. wrote the paper. N.H. directed and supervised the work.

ACKNOWLEDGMENTS

We thank Dr. Y. Noda for the KIF2A antibody and Dr. N. Homma for the *Kif2a*$^{-/-}$ mice. We thank Dr. Y. Okada, Dr. Y. Tanaka, and all the members of the N.H. laboratory for valuable discussions and help. We thank Ms. H. Sato, Ms. H. Fukuda, Mr. T. Akamatsu, and Mr. N. Onouchi for technical assistance. We also thank Drs. G. Marko-Varga, T. Nishimura, T. Kasama, Y. Oda, H. Kawakami, J. Kamiie, Y. Bando, and H. Kosako for their valuable discussions and help. This work was supported by the Japan Electron Optics Laboratory, Carl Zeiss, the Global Centers of Excellence Program, and a Grant-in-Aid for Specially Promoted Research by the Ministry of Education, Culture, Sports, Science, and Technology of Japan to N.H. This work was partly supported by the Grant-in-Aid for JSPS Fellows under grant no. 05J11417 to T.O.

Received: October 24, 2014
Revised: June 2, 2015
Accepted: August 4, 2015
Published: September 3, 2015

REFERENCES

Aizawa, H., Sekine, Y., Takemura, R., Zhang, Z., Nangaku, M., and Hirokawa, N. (1992). Kinesin family in murine central nervous system. J. Cell Biol. *119*, 1287–1296.

Bito, H., Furuyashiki, T., Ishihara, H., Shibasaki, Y., Ohashi, K., Mizuno, K., Maekawa, M., Ishizaki, T., and Narumiya, S. (2000). A critical role for a Rho-associated kinase, p160ROCK, in determining axon outgrowth in mammalian CNS neurons. Neuron *26*, 431–441.

Cau, J., and Hall, A. (2005). Cdc42 controls the polarity of the actin and microtubule cytoskeletons through two distinct signal transduction pathways. J. Cell Sci. *118*, 2579–2587.

Cheung, Z.H., Chin, W.H., Chen, Y., Ng, Y.P., and Ip, N.Y. (2007). Cdk5 is involved in BDNF-stimulated dendritic growth in hippocampal neurons. PLoS Biol. *5*, e63.

Daub, H., Gevaert, K., Vandekerckhove, J., Sobel, A., and Hall, A. (2001). Rac/Cdc42 and p65PAK regulate the microtubule-destabilizing protein stathmin through phosphorylation at serine 16. J. Biol. Chem. *276*, 1677–1680.

Desai, A., Verma, S., Mitchison, T.J., and Walczak, C.E. (1999). Kin I kinesins are microtubule-destabilizing enzymes. Cell *96*, 69–78.

Hertzer, K.M., and Walczak, C.E. (2008). The C-termini of tubulin and the specific geometry of tubulin substrates influence the depolymerization activity of MCAK. Cell Cycle *7*, 2727–2737.

Hertzer, K.M., Ems-McClung, S.C., Kline-Smith, S.L., Lipkin, T.G., Gilbert, S.P., and Walczak, C.E. (2006). Full-length dimeric MCAK is a more efficient microtubule depolymerase than minimal domain monomeric MCAK. Mol. Biol. Cell *17*, 700–710.

Hirokawa, N. (1997). The mechanisms of fast and slow transport in neurons: identification and characterization of the new kinesin superfamily motors. Curr. Opin. Neurobiol. *7*, 605–614.

Hirokawa, N. (1998). Kinesin and dynein superfamily proteins and the mechanism of organelle transport. Science *279*, 519–526.

Hirokawa, N., Niwa, S., and Tanaka, Y. (2010). Molecular motors in neurons: transport mechanisms and roles in brain function, development, and disease. Neuron *68*, 610–638.

Homma, N., Takei, Y., Tanaka, Y., Nakata, T., Terada, S., Kikkawa, M., Noda, Y., and Hirokawa, N. (2003). Kinesin superfamily protein 2A (KIF2A) functions in suppression of collateral branch extension. Cell *114*, 229–239.

Hunter, A.W., Caplow, M., Coy, D.L., Hancock, W.O., Diez, S., Wordeman, L., and Howard, J. (2003). The kinesin-related protein MCAK is a microtubule depolymerase that forms an ATP-hydrolyzing complex at microtubule ends. Mol. Cell *11*, 445–457.

Kinoshita, E., Kinoshita-Kikuta, E., Takiyama, K., and Koike, T. (2006). Phosphate-binding tag, a new tool to visualize phosphorylated proteins. Mol. Cell. Proteomics *5*, 749–757.

Lan, W., Zhang, X., Kline-Smith, S.L., Rosasco, S.E., Barrett-Wilt, G.A., Shabanowitz, J., Hunt, D.F., Walczak, C.E., and Stukenberg, P.T. (2004). Aurora B phosphorylates centromeric MCAK and regulates its localization and microtubule depolymerization activity. Curr. Biol. *14*, 273–286.

Lawrence, C.J., Dawe, R.K., Christie, K.R., Cleveland, D.W., Dawson, S.C., Endow, S.A., Goldstein, L.S.B., Goodson, H.V., Hirokawa, N., Howard, J., et al. (2004). A standardized kinesin nomenclature. J. Cell Biol. *167*, 19–22.

Maney, T., Wagenbach, M., and Wordeman, L. (2001). Molecular dissection of the microtubule depolymerizing activity of mitotic centromere-associated kinesin. J. Biol. Chem. *276*, 34753–34758.

Miki, H., Setou, M., Kaneshiro, K., and Hirokawa, N. (2001). All kinesin superfamily protein, KIF, genes in mouse and human. Proc. Natl. Acad. Sci. USA *98*, 7004–7011.

Moore, A., and Wordeman, L. (2004). C-terminus of mitotic centromere-associated kinesin (MCAK) inhibits its lattice-stimulated ATPase activity. Biochem. J. *383*, 227–235.

Moores, C.A., Yu, M., Guo, J., Beraud, C., and Sakowicz, R. (2002). A mechanism for microtubule depolymerization by KinI kinesins. Mol. Cell *9*, 903–909.

Nikolic, M., Dudek, H., Kwon, Y.T., Ramos, Y.F., and Tsai, L.H. (1996). The cdk5/p35 kinase is essential for neurite outgrowth during neuronal differentiation. Genes Dev. *10*, 816–825.

Noda, Y., Sato-Yoshitake, R., Kondo, S., Nangaku, M., and Hirokawa, N. (1995). KIF2 is a new microtubule-based anterograde motor that transports membranous organelles distinct from those carried by kinesin heavy chain or KIF3A/B. J. Cell Biol. *129*, 157–167.

Noda, Y., Niwa, S., Homma, N., Fukuda, H., Imajo-Ohmi, S., and Hirokawa, N. (2012). Phosphatidylinositol 4-phosphate 5-kinase alpha (PIPKα) regulates neuronal microtubule depolymerase kinesin, KIF2A and suppresses elongation of axon branches. Proc. Natl. Acad. Sci. USA *109*, 1725–1730.

Ogawa, T., Nitta, R., Okada, Y., and Hirokawa, N. (2004). A common mechanism for microtubule destabilizers-M type kinesins stabilize curling of the protofilament using the class-specific neck and loops. Cell *116*, 591–602.

Ohi, R., Sapra, T., Howard, J., and Mitchison, T.J. (2004). Differentiation of cytoplasmic and meiotic spindle assembly MCAK functions by Aurora B-dependent phosphorylation. Mol. Biol. Cell *15*, 2895–2906.

Patrick, G.N., Zukerberg, L., Nikolic, M., de la Monte, S., Dikkes, P., and Tsai, L.H. (1999). Conversion of p35 to p25 deregulates Cdk5 activity and promotes neurodegeneration. Nature *402*, 615–622.

Picotti, P., Rinner, O., Stallmach, R., Dautel, F., Farrah, T., Domon, B., Wenschuh, H., and Aebersold, R. (2010). High-throughput generation of selected reaction-monitoring assays for proteins and proteomes. Nat. Methods *7*, 43–46.

Riento, K., and Ridley, A.J. (2003). Rocks: multifunctional kinases in cell behaviour. Nat. Rev. Mol. Cell Biol. *4*, 446–456.

Shipley, K., Hekmat-Nejad, M., Turner, J., Moores, C., Anderson, R., Milligan, R., Sakowicz, R., and Fletterick, R. (2004). Structure of a kinesin microtubule depolymerization machine. EMBO J. *23*, 1422–1432.

Takenawa, T., and Miki, H. (2001). WASP and WAVE family proteins: key molecules for rapid rearrangement of cortical actin filaments and cell movement. J. Cell Sci. *114*, 1801–1809.

van Horck, F.P.G., Lavazais, E., Eickholt, B.J., Moolenaar, W.H., and Divecha, N. (2002). Essential role of type I(alpha) phosphatidylinositol 4-phosphate 5-kinase in neurite remodeling. Curr. Biol. *12*, 241–245.

Walczak, C.E., Mitchison, T.J., and Desai, A. (1996). XKCM1: a Xenopus kinesin-related protein that regulates microtubule dynamics during mitotic spindle assembly. Cell *84*, 37–47.

Walther, T.C., and Mann, M. (2010). Mass spectrometry-based proteomics in cell biology. J. Cell Biol. *190*, 491–500.

Wordeman, L., and Mitchison, T.J. (1995). Identification and partial characterization of mitotic centromere-associated kinesin, a kinesin-related protein that associates with centromeres during mitosis. J. Cell Biol. *128*, 95–104.